

Confidence Tubes for Curves on $SO(3)$ and Identification of Subject-Specific Gait Change after Kneeling

Fabian J.E. Telschow*, Michael R. Pierrynowski† and Stephan F. Huckemann‡

Abstract

In order to identify changes of gait patterns, e.g. due to prolonged occupational kneeling, which is believed to be major risk factor, among others, for the development of knee osteoarthritis, we develop confidence tubes for curves following a Gaussian perturbation model on $SO(3)$. These are based on an application of the Gaussian kinematic formula to a process of Hotelling statistics and we approximate them by a computable version, for which we show convergence. Simulations endorse our method, which in application to gait curves from eight volunteers undergoing kneeling tasks, identifies phases of the gait cycle that have changed due to kneeling tasks. We find that after kneeling, deviation from normal gait is stronger, in particular for older aged male volunteers. Notably our method adjusts for different walking speeds and marker replacement at different visits.

Keywords: Functional data analysis, modulo group actions, Gaussian perturbation models, Gaussian kinematic formula, two-sample tests, Lie groups

1 Introduction

There is overwhelming evidence that *prolonged occupational kneeling* (POK), e.g. floor tile laying, constitutes a major risk factor for the development of knee osteoarthritis, e.g. Cooper et al. (1994); Coggon et al. (2000); Rytter et al. (2009). Also, POK is a risk factor for the development of degenerative tears in medial menisci, e.g. Rytter et al. (2009). In order to identify hypothesized underlying changes of gait patterns, kneeling workers' and controls' gait has been compared by Gaudreault et al. (2013) and prolonged kneeling has been *simulated* and gait changes compared by Kajaks and Costigan (2015); Tennant et al. (2018). Also, dependence of kneeling effects due to footwear has been investigated by Tennant et al. (2015) and kneeling effects have been studied on cadavers with total knee arthroplasty Wilkens et al. (2007).

In order to assess the specifics of changes of gait patterns, the three dimensional rotational path in $SO(3)$ of the relative motion of the tibia (larger lower leg bone) w.r.t. the femur (upper leg bone) is usually represented by the three Euler angles flexion/extension, adduction/abduction and internal/external rotation. Doing so, Gaudreault et al. (2013); Kajaks and Costigan (2015); Tennant et al. (2018) have found, among others, for each angle, loci of significant gait changes, without, however, addressing the issue of multiple testing, correlation of the sequential data and the effect of marker replacement.

In our approach, we address all of these issues, and in consequence, are able to test for subject-specific changes of gait pattern. In application, we do this for pre- and post-kneeling, the method, however, is applicable for any change of condition (e.g. onset of otheoarthritis) over a period of time, due to correcting for marker replacement. To this end, we recall a Gaussian perturbation model from Telschow et al. (2016) for curves on Lie groups and show that a Hotelling statistic for the corresponding process follows asymptotically (for vanishing variance) a Hotelling statistic

*Division of Biostatistics, University of California, San Diego

†School of Rehabilitation Science, McMaster University, Canada

‡Felix Bernstein Institute for Mathematical Statistics in the Biosciences, Georgia Augusta University of Göttingen

that can be described by a *Gaussian kinematic formula* (GFK) from Taylor et al. (2005); Taylor (2006). In application to gait analysis, our method, relying on curves on the rotational group, takes advantage of simultaneously involving all three Euler angles in a canonical way. Moreover, as our test statistics use maxima of stochastic processes, we resolve the multiple testing issue by providing for simultaneous confidence tubes over entire gait cycles. Further, sequential correlation is naturally modeled within the GFK approach by simulating quantiles from the empirical process. Indeed, simulations mimicking and going beyond the use case of low variance and high smoothness typical in gait analysis show that our method is well applicable. Then, for an experiment conducted in the School of Rehabilitation Science at McMaster University (Canada), for six out of eight healthy volunteers we identify individual changes of gait patterns after kneeling tasks. We find that after kneeling, deviation from normal gait is stronger, in particular for older aged male volunteers.

Remarkably, our method is also robust under specialist marker replacement, at a subsequent patient's visit, say. It is well known that Euler angle curves may considerably change after marker replacement and simple approaches subtracting average angles over gait cycles (cf. Kadaba et al. (1989)) have remained questionable, e.g. Delval et al. (2008); McGinley et al. (2009); Noehren et al. (2010); Røislien et al. (2012), also for other approaches, leading to the longstanding open problem of *gait reproducibility*, see Duhamel et al. (2004).

In a recent publication (Telschow et al. (2016)), we have developed a method to successfully correct for marker replacement by estimating a Lie group isometry, bringing two samples (each sample is a repeated measurement of the same person's gait with fixed marker placement) into optimal position to one another. Since volunteers will have different comfortable walking speeds at different visits, we have also corrected for a sample-specific time warping effect. This method is part of the tool chain developed in the present contribution which is available under www.stochastik.math.uni-goettingen.de/KneeMotionAnalytics as an R-package. In particular, it contains all data and code used in this paper.

2 Testing Gaussian Perturbation Models on Lie Groups Modulo Sample-Specific Spatio-Temporal Action

The following is taken, from Telschow et al. (2016). It has been formulated for $p = 1$ and generalizes at once to arbitrary $p \in \mathbb{N}$. Let G be a connected Lie group with Lie algebra \mathfrak{g} embedded in a suitable Euclidean space \mathbb{R}^m and Lie exponential $\text{Exp} : \mathfrak{g} \rightarrow G$. With the unit interval $I = [0, 1]$ we have the family $\Gamma = \mathcal{C}^p([0, 1], G)$ of $p \in \mathbb{N}$ times continuously differentiable curves on G . We assume in particular that G admits a bi-invariant Riemannian metric, a sufficient condition for which is that G is compact.

Definition 2.1. *We say that a random curve $\gamma \in \Gamma$ follows a Gaussian perturbation (GP) around a center curve $\gamma_0 \in \Gamma$ if there is a \mathfrak{g} -valued zero-mean Gaussian process A_t with a.s. \mathcal{C}^p paths, such that*

$$\gamma(t) = \gamma_0(t)\text{Exp}(A_t) \text{ for all } t \in I. \quad (1)$$

The Gaussian process A_t will be called the generating process.

This model, which is based on right multiplication with the exponential of the generating process is equivalent to one based on left multiplication and asymptotically (as the variance goes to zero) equivalent to one based on two-sided multiplication, cf. Telschow et al. (2016). Moreover, this model is invariant under the *spatial* action of the isometry group $\mathcal{I}(G)$ on G , where its connectivity component $\mathcal{I}_0(G)$ of the identity element can be viewed as the analog of the orientation preserving Euclidean motions of a Euclidean space. Indeed, for G compact, semisimple with trivial center, we have $G \times G = \mathcal{I}_0(G)$, cf. Telschow et al. (2016), which is the case for $G = SO(3)$.

Also, Model (1) is invariant under the temporal action

$$\phi \in \text{Diff}^+(I) = \{\phi \in \mathcal{C}^\infty(I, I) : \phi'(t) > 0 \text{ for all } t \in I\}$$

of strictly monotone time warpings. We set $\mathcal{S} = \mathcal{I}_0(G) \times \text{Diff}^+(\mathbb{I})$ and write $(\psi, \phi) : \gamma \mapsto \psi \circ \gamma \circ \phi$ for the corresponding action on Γ , $\psi \in \mathcal{I}_0(G)$ and $\phi \in \text{Diff}^+(\mathbb{I})$.

If G admits a bi-invariant Riemannian metric (it does, if it is compact, say), on Γ we introduced the *intrinsic length loss*

$$\delta(\gamma, \eta) = \frac{1}{2}(\delta_1(\gamma, \eta) + \delta_2(\gamma, \eta)).$$

where

$$\delta_1(\gamma, \eta) = \text{length}(\gamma\eta^{-1}) \quad \text{and} \quad \delta_2(\gamma, \eta) = \text{length}(\gamma^{-1}\eta),$$

for $\gamma, \eta \in \Gamma$. Here, the length is taken with respect to the bi-invariant metric on G ,

$$\text{length}(\gamma) = \int_0^1 \|\dot{\gamma}(t)\| dt$$

The loss δ is invariant under the spatio-temporal action. There are other loss functions, canonical on Euclidean space modulo time warping, that can be extended to manifolds, cf. Srivastava et al. (2011); Su et al. (2014).

For independent i.i.d. samples $\chi_1 = \{\gamma_1, \dots, \gamma_N\}$ and $\chi_2 = \{\eta_1, \dots, \eta_M\}$, $N, M \in \mathbb{N}$, of GP models γ and η with center curves γ_0 and η_0 , respectively, we have developed in Telschow et al. (2016) rank permutation tests for

$$H_0 : \exists(\psi, \phi) \in \mathcal{S} : \gamma \sim \psi \circ \eta \circ \phi \quad \text{vs.} \quad H_1 : \forall(\psi, \phi) \in \mathcal{S} : \gamma \not\sim \psi \circ \eta \circ \phi \quad (2)$$

at a given significance level $\alpha \in (0, 1)$. Notably, in contrast to classical shape analysis correcting for group action on individual measurements, we correct for a common *sample-specific group action* and to this end, in application in Section 6, we apply Telschow et al. (2016, Test 2.11).

3 Confidence Tubes on G

Since G is connected by hypothesis, the inverse exponential is well defined on the complement in G of the cut locus of the unit element. Let $\text{Log} : G \rightarrow \mathfrak{g}$ denote a measurable extension. Further, since \mathfrak{g} is a linear space, let $\iota : \mathbb{R}^m \rightarrow \mathfrak{g}$ be a suitable isomorphism and set $\mathfrak{L} = \iota^{-1} \circ \text{Log} : G \rightarrow \mathbb{R}^m$.

Definition 3.1. *Let $\gamma_1, \dots, \gamma_N$ be a sample of a random curve $\gamma \in \Gamma$ following a GP model around a center curve γ_0 and let $\hat{\gamma}_N$ be an estimator for γ_0 . Then*

$$x_t^N = \mathfrak{L}\left(\hat{\gamma}_N^{-1}(t)\gamma_0(t)\right), \quad (3)$$

$$x_t^{N,n} = \mathfrak{L}\left(\hat{\gamma}_N^{-1}(t)\gamma_n(t)\right) \quad (4)$$

are called *intrinsic population and sample residuals, respectively*.

This gives rise to the following one-dimensional processes,

$$\hat{H}_t^{x,N} = N(x_t^N)^T \left(\hat{S}_t^{x,N}\right)^{-1} x_t^N, \quad \text{where} \quad \hat{S}_t^{x,N} = \frac{1}{N-1} \sum_{n=1}^N x_t^{N,n} (x_t^{N,n})^T, \quad (5)$$

where we assume that $\hat{S}_t^{x,N}$ is non-singular for all $t \in [0, 1]$. Further, for $0 \leq \alpha \leq 1$ we define the quantile

$$\hat{h}_{\gamma,N,\alpha} = \inf \left\{ h \in \mathbb{R}_{\geq 0} \mid \mathbb{P} \left\{ \sup_{t \in [0,1]} \hat{H}_t^{x,N} \leq h \right\} \geq 1 - \alpha \right\}.$$

From this we obtain at once simultaneous $(1 - \alpha)$ -confidence tubes for γ_0 , setting

$$\mathcal{V}_\alpha(\gamma_1, \dots, \gamma_N; t) = \left\{ a \in \mathfrak{g} \mid Na^T \left(\hat{S}_t^{x,N}\right)^{-1} a \leq \hat{h}_{\gamma,N,\alpha} \right\}.$$

Theorem 3.2. Let $\gamma_1, \dots, \gamma_N$ be a sample of a random curve $\gamma \in \Gamma$ following a GP model around a center curve γ_0 . Let $\hat{\gamma}_N$ be an estimator for γ_0 and assume $\hat{S}_t^{x,N}$ is non-singular for all $t \in [0, 1]$. Then

$$\mathbb{P}\left\{\gamma_0(t) \in \hat{\gamma}_N(t) \text{ Exp}\left(\iota \circ \mathcal{V}_\alpha(\gamma_1, \dots, \gamma_N; t)\right) \text{ for all } t \in [0, 1]\right\} \geq \alpha$$

and hence this set forms a simultaneous $(1 - \alpha)$ -confidence tube for γ_0 .

The process $\hat{H}_t^{x,N}$ from (5) serves as an approximation of the genuine Hotelling process determined by (1):

$$H_t^{a,N} = N (\bar{a}_t^N)^T (S_t^{a,N})^{-1} \bar{a}_t^N \quad (6)$$

where $\gamma_n(t) = \gamma_0 \text{Exp}(A_t^n)$, $\mathbb{E}[A_t^n] = 0$ for $1 \leq n \leq N$ and $t \in I$, as well as,

$$\iota^{-1} \circ A_t^n = a_t^n, \quad \bar{a}_t^N = \frac{1}{N} \sum_{n=1}^N a_t^n \quad \text{and} \quad S_t^{a,N} = \frac{1}{N-1} \sum_{n=1}^N (a_t^n - \bar{a}_t^N)(a_t^n - \bar{a}_t^N)^T. \quad (7)$$

Among others, the following section makes this approximation explicit for the special case of $G = SO(3)$.

4 GP Models and Approximating Confidence Tubes on $SO(3)$

For G , the compact and connected Lie group of three-dimensional rotations $G = SO(3)$ we detail the above approximation. To this end, we first recall the structure of $SO(3)$, extrinsic pointwise means as estimators $\hat{\gamma}_N$ and fundamental properties of corresponding GP models.

4.1 GP Models on $SO(3)$

The Lie group $G = SO(3)$ comes with the Lie algebra $\mathfrak{g} = \mathfrak{so}(3) = \{A \in \mathbb{R}^{3 \times 3} : A^T = -A\}$ of 3×3 skew symmetric matrices. This Lie algebra is a three-dimensional linear subspace of all 3×3 matrices and thus carries the natural structure of \mathbb{R}^3 conveyed by the isomorphism $\iota : \mathbb{R}^3 \rightarrow \mathfrak{so}(3)$ given by

$$\iota(a) = \begin{pmatrix} 0 & -a_3 & a_2 \\ a_3 & 0 & -a_1 \\ -a_2 & a_1 & 0 \end{pmatrix}, \quad \text{for } a = (a_1, a_2, a_3)^T \in \mathbb{R}^3.$$

This isomorphism exhibits at once the following relation

$$Q\iota(a)Q^T = \iota(Qa) \text{ for all } a \in \mathbb{R}^3 \text{ and } Q \in G. \quad (8)$$

We use the scalar product $\langle A, B \rangle := \text{trace}(AB^T)/2 = a^T b$ for $\iota^{-1}(A) = a$ and $\iota^{-1}(B) = b$, which induces the rescaled Frobenius norm $\|A\|_F = \sqrt{\text{trace}(AA^T)/2} = \|a\|$, on all $\mathbb{R}^{3 \times 3}$. On $G \subset \mathbb{R}^{3 \times 3}$ it induces the *extrinsic metric*, cf. Bhattacharya and Patrangenaru (2003). Moreover, we denote with $I_{3 \times 3}$ the unit matrix. As usual, $A \mapsto \text{Exp}(A)$ denotes the matrix exponential which is identical to the Lie exponential and gives a surjection $\mathfrak{g} \rightarrow G$. Due to skew symmetry, the following *Rodriguez formula* holds

$$\text{Exp}(A) = \sum_{j=0}^{\infty} \frac{A^j}{j!} = I_{3 \times 3} + \frac{\sin(\|A\|_F)}{\|A\|_F} A + \frac{1 - \cos(\|A\|_F)}{\|A\|_F^2} A^2. \quad (9)$$

This yields that the Lie exponential is bijective on $\mathcal{B}_\pi(0) = \{A \in \mathfrak{g} : \|A\|_F < \pi\}$. For a detailed discussion, see (Chirikjian and Kyatkin 2000, p. 121).

As in Telschow et al. (2016), introduce *pointwise extrinsic mean* (PEM) curves $\hat{\gamma}_N(t)$ of a sample $\gamma_1, \dots, \gamma_N \stackrel{i.i.d.}{\sim} \gamma \in \Gamma$, which are defined for each $t \in [0, 1]$ by

$$\hat{\gamma}_N(t) \in \hat{E}_N(t) = \underset{\mu \in G}{\text{argmin}} \frac{1}{N} \sum_{n=1}^N \|\mu - \gamma_n(t)\|_F^2. \quad (10)$$

They fulfill the following uniqueness and convergence properties for GP models as proven in Telschow et al. (2016).

Theorem 4.1. *Let $\gamma_1, \dots, \gamma_N$ be a sample of a random curve $\gamma \in \Gamma$ following a GP model around a center curve γ_0 and let $t \mapsto \hat{\gamma}_N(t)$ be a measurable selection of $\hat{E}_N(t)$ for each time point $t \in [0, 1]$. If the generating Gaussian process A_t satisfies*

$$\mathbb{E} \left[\max_{t \in [0,1]} \|\partial_t A_t\|_F \right] < \infty, \quad (11)$$

then the following hold.

- (i) *There is $\Omega' \subset \Omega$ measurable with $\mathbb{P}(\Omega') = 1$ such that for every $\omega \in \Omega'$ there is $N_\omega \in \mathbb{N}$ such that for all $N \geq N_\omega$, every $\hat{E}_N(t)$ has a unique element $\hat{\gamma}_N(t)$, for all $t \in [0, 1]$, and $\hat{\gamma}_N \in \Gamma$;*
- (ii) *$\max_{t \in [0,1]} \|\hat{\gamma}_N(t) - \gamma_0(t)\|_F \rightarrow 0$ for $N \rightarrow \infty$ almost surely.*

Corollary 4.2. *With the notations and assumptions of Theorem 4.1 we have*

$$\lim_{N \rightarrow \infty} \mathbb{P}\{t \mapsto \hat{\gamma}_N(t) \in \Gamma\} = 1.$$

4.2 Approximating Confidence Tubes on $SO(3)$

As the main result of this section we first show that in case of concentrated errors (as is typical in biomechanics, e.g. Rancourt et al. (2000)), the residual processes x_t^N and $X_t^{N,n}$ from Definition 3.1 are approximatively the residuals of the generating Gaussian process (7) of the GP model. Then, we use this approximation to define an estimator for $\hat{h}_{\gamma, N, \alpha}$ based on the Gaussian kinematic formula for Hotelling processes (see Taylor and Worsley (2008)), which will be shown in Section 5, using simulations, to perform very reliably even if the sample sizes are small as it is usually the case in biomechanical gait analysis.

Theorem 4.3 (Approximations for Concentrated Errors). *Let $N \in \mathbb{N}$ be fixed and $\gamma_1, \dots, \gamma_N$ be a sample of a random curve $\gamma \in \Gamma$ following a GP model around a center curve γ_0 . Additionally, assume that the generating Gaussian process $A_t = \iota \circ a_t$ satisfies $\mathbb{E} [\max_{t \in [0,1]} \|\partial_t A_t\|_F] < \infty$ and $\max_{t \in [0,1]} \|A_t\|_F = \mathcal{O}_p(\sigma)$ with $0 < \sigma \rightarrow 0$. Let $\hat{\gamma}_N(t)$ be a measurable selection of sample PEM curves. Then, for x_t^N and $x_t^{N,n}$ from Definition 3.1,*

$$x_t^N = \bar{a}_t^N + \mathcal{O}_p(\sigma^2) \quad (12)$$

$$x_t^{N,n} = a_t^n - \bar{a}_t^N + \mathcal{O}_p(\sigma^2), \quad (13)$$

where $\mathcal{O}_p(\sigma^2)$ is uniform over $t \in [0, 1]$.

Corollary 4.4 (Asymptotically genuine Hotelling process). *With the assumptions and notations of Theorem 4.3 we obtain with $\mathcal{O}_p(\sigma)$ uniformly over $t \in [0, 1]$,*

$$H_t^{a,N} = \hat{H}_t^{x,N} + \mathcal{O}_p(\sigma),$$

if additionally $\text{cov}[a_t] = \sigma^2 \Sigma_t$ with fixed and non-singular Σ_t for all $t \in [0, 1]$.

The following theorem gives the equivariance property of the simultaneous confidence tubes with respect to the group action on Γ of the group $\mathcal{I}_0(G) \times \text{Diff}^+(I)$, which is $(G \times G) \times \text{Diff}^+(I)$ by Section 2.

Theorem 4.5. *Let $\gamma_1, \dots, \gamma_N$ be a sample of a random curve $\gamma \in \Gamma$ following a GP model around a center curve γ_0 with PEM curve $\hat{\gamma}_N$. Moreover, let $(\psi, \phi) \in (G \times G) \times \text{Diff}^+(I)$ be arbitrary and define the sample $\eta_n = \psi \circ \gamma_n \circ \phi$, $n \in \{1, \dots, N\}$ of the GP $\psi \circ \gamma \circ \phi$ with center curve*

$\eta_0 = \psi \circ \gamma_0 \circ \phi$ and PEM curve $\hat{\eta}_N$. Then, for every $0 \leq \alpha \leq 1$, the simultaneous confidence tubes for $\psi \circ \gamma_0 \circ \phi$ computed from η_1, \dots, η_N satisfy

$$\hat{\eta}_N(t) \text{Exp}\left(\iota \circ \mathcal{V}_\alpha(\eta_1, \dots, \eta_N; t)\right) = (\psi \circ \hat{\gamma}_N \circ \phi)(t) \text{Exp}\left(\iota \circ Q_\psi \mathcal{V}_\alpha(\gamma_1, \dots, \gamma_N; \phi(t))\right),$$

i.e., they can be derived from the simultaneous confidence tubes for γ_0 using $\gamma_1, \dots, \gamma_N$ and $(\psi, \phi) \in (G \times G) \times \text{Diff}^+(\mathbf{I})$ only.

The Gaussian kinematic formula (GKF). Corollary 4.4 states that for concentrated errors the statistic H_t^a , which is the Hotelling T^2 statistic of a generating Gaussian process, approximates the statistic $\hat{H}_t^{x,N}$. Thus, in order to estimate the quantiles $\hat{h}_{\gamma,N,\alpha}$ for the process $\hat{H}_t^{x,N}$, derived from a GP model γ , we use the *expected Euler characteristic heuristic* (see Taylor et al. (2005)) and assume that

$$\mathbb{P}\left(\max_{t \in [0,1]} \hat{H}_t^{x,N} > h\right) \approx \mathbb{E}\left[\mathfrak{r}\left(\left\{t \in [0,1] \mid \hat{H}_t^{x,N} \geq h\right\}\right)\right] \approx \mathbb{E}\left[\mathfrak{r}\left(\left\{t \in [0,1] \mid H_t^{a,N} \geq h\right\}\right)\right], \quad (14)$$

where $\mathfrak{r}(\mathcal{U})$ denotes the *Euler characteristic* (EC) of $\mathcal{U} \subset [0,1]$. Although we cannot rigorously justify this approximation, our simulations in Section 5 show that this procedure works very well.

Under some additional technical assumptions on the generating Gaussian process $A_t = \iota \circ a_t$ given in Taylor (2006), it is shown in Taylor and Worsley (2008) that the expected EC of the excursion set $\left\{t \in [0,1] \mid H_t^{a,N} \geq h\right\}$ can be computed explicitly by the formula

$$\mathbb{E}\left[\mathfrak{r}\left\{t \in [0,1] \mid H_t^{a,N} \geq h\right\}\right] = \mathcal{L}_0([0,1])\rho_0^H(h) + \mathcal{L}_1([0,1])\rho_1^H(h) \quad (15)$$

with the so called Lipschitz-Killing curvatures

$$\mathcal{L}_0([0,1]) = 1, \quad \mathcal{L}_1([0,1]) = \int_0^1 \sqrt{\text{var}\left[\frac{da}{dt}(t)\right]} dt.$$

The so called *Euler characteristic densities* ρ_j^H for $j \in \{1,2\}$ appearing in the GKF (15) can be computed from the EC densities of a T -process with $N-1$ degrees of freedom via Roy's union intersection principle (cf. Taylor and Worsley (2008, Sec. 3.1.)) using the formula

$$\rho_j^H(h) = \sum_{d=1}^3 \mu_d(S^2) \rho_{j+d}^T(\sqrt{h}), \quad j = 0, 1.$$

Here $\mu_d(S^2)$ denotes the d -dimensional intrinsic volume of the two-sphere S^2 given by

$$\mu_0(S^2) = 2, \quad \mu_1(S^2) = 0 = \mu_3(S^2), \quad \mu_2(S^2) = 4\pi,$$

in Taylor and Worsley (2008, p. 23). In relation to the Stochastic Geometry literature, μ_0 gives twice the number of connected components and μ_2 gives the surface area of S^2 (e.g., Mecke and Stoyan (2000, p. 100)). Moreover, the EC densities of a T -process with $(N-1)$ degrees of freedom have the explicit representations

$$\begin{aligned} \rho_0^T(t) &= \int_t^\infty \frac{\Gamma\left(\frac{N}{2}\right)}{\sqrt{N-1}\pi\Gamma\left(\frac{N-1}{2}\right)} \left(1 + \frac{u^2}{N-1}\right)^{-N/2} du \\ \rho_1^T(t) &= (2\pi)^{-1} \left(1 + \frac{t^2}{N-1}\right)^{1-N/2} \\ \rho_2^T(t) &= (2\pi)^{-3/2} \frac{\Gamma\left(\frac{N}{2}\right)}{\sqrt{\frac{N-1}{2}}\Gamma\left(\frac{N-1}{2}\right)} t \left(1 + \frac{t^2}{N-1}\right)^{1-N/2} \\ \rho_3^T(t) &= (2\pi)^{-2} \left(\frac{N-2}{N-1}t^2 - 1\right) \left(1 + \frac{t^2}{N-1}\right)^{1-N/2}, \end{aligned}$$

given in Taylor and Worsley (2007, p. 915).

Estimation of the quantile $\hat{h}_{\gamma, N, \alpha}$. Using the GKF for Hotelling T^2 -processes together with the EC heuristic (14) yields

$$\mathbb{P}\left(\max_{t \in [0, 1]} \hat{H}_t^{x, N} > h\right) \approx 2\rho_0^T(\sqrt{h}) - 4\pi\rho_2^T(\sqrt{h}) - \mathcal{L}_1([0, 1]) \left(2\rho_1^T(\sqrt{h}) + 4\pi\rho_3^T(\sqrt{h})\right),$$

which can be used if $\mathcal{L}_1([0, 1])$ is known, to estimate the value $\hat{h}_{\alpha, N, \alpha}$ for low probabilities α by solving

$$2\rho_0^T(\sqrt{h}) - 4\pi\rho_2^T(\sqrt{h}) - \mathcal{L}_1([0, 1]) \left(2\rho_1^T(\sqrt{h}) + 4\pi\rho_3^T(\sqrt{h})\right) = 1 - \alpha. \quad (16)$$

Thus, it remains to estimate the Lipschitz-Killing curvature $\mathcal{L}_1([0, 1])$. This has been achieved for Gaussian processes in \mathbb{R}^D , $D \in \mathbb{N}$, in Taylor and Worsley (2007, Sect. 4) and Taylor and Worsley (2008), where they also proved that their estimator is consistent.

By Theorem 4.3 the intrinsic residuals of a sample from a GP model γ are, in case of concentrated errors, close to the residuals of the generating Gaussian process $A_t = \iota \circ a_t$. Since the estimator of Taylor and Worsley (2008, Equation (18)) is based only on the Gaussian residuals, we adapt their estimator by replacing their residuals by the intrinsic residuals given in Theorem 4.3 to obtain an estimator of the Lipschitz-Killing curvature $\mathcal{L}_1([0, 1])$.

For convenience we restate the resulting estimator. Let $\gamma_1, \dots, \gamma_N$ be a sample of a GP model γ and assume the curves are observed at times $0 = t_1 < t_2 < \dots < t_K = 1$. Then we define the matrix

$$R_{t_k} = (X_{t_k}^1, \dots, X_{t_k}^N)^T \in \mathbb{R}^{N \times 3}.$$

Further, denote by $R_{t_k}^d$ the d -th column of R_{t_k} and define the normalized residuals as

$$\hat{R}_{t_k}^d = \frac{R_{t_k}^d}{\|R_{t_k}^d\|}$$

for $d \in \{1, 2, 3\}$ and $k \in \{1, \dots, K\}$. The estimator of the Lipschitz-Killing curvature $\mathcal{L}_1([0, 1])$ is then given by

$$\hat{\mathcal{L}}_1(I) = \frac{1}{3} \sum_{k=1}^{K-1} \sum_{d=1}^3 \|\hat{R}_{t_{k+1}}^d - \hat{R}_{t_k}^d\|. \quad (17)$$

5 Simulations of Covering Rates

Since the estimation of the quantile $\hat{h}_{\gamma, N, \alpha}$ relies on an approximation for concentrated error processes given in Theorem 4.3, we study the actual covering rate of this method using simulations.

GP models used for simulation. Without loss of generality we may assume that our center curves satisfy $\gamma_0(t) = I_{3 \times 3}$ for all $t \in [0, 1]$. Otherwise, multiply the sample with $\gamma_0(t)^{-1}$.

In our simulations studying the covering rates of the simultaneous confidence sets given in Theorem 3.2, we use the error processes

$$\begin{aligned} \varepsilon_t^{1,l} &= f_l(t) \left(b_1 \sin\left(\frac{\pi}{2}t\right) + b_2 \cos\left(\frac{\pi}{2}t\right) \right) \\ \varepsilon_t^{2,l} &= f_l(t) \left(\frac{\sum_{i=1}^{10} b_i e^{-\frac{(x - \frac{i-1}{9})^2}{0.2}}}{\sqrt{\sum_{i=1}^{10} e^{-\frac{(x - \frac{i-1}{9})^2}{0.2}}}} \right) \\ \varepsilon_t^{3,l} &= f_l(t) \left(b_0 e^{-5t} + \sqrt{10} \int_0^t e^{5(s-t)} dW_t \right) \end{aligned} \quad (18)$$

with i.i.d. $b_i \sim \mathcal{N}(0, 1)$ for $i \in \{0, \dots, 10\}$, $\{W_t\}_{t \in I}$ a Wiener process, and for $l \in \{1, 2, 3\}$ we set

$$f_1(t) = 1, \quad f_2(t) = 4, \quad f_3(t) = \sin(4\pi t) + 1.5.$$

Note that the processes satisfy $\text{var}[\varepsilon_t^{\nu,l}] = f_l(t)^2$ for all $t \in [0, 1]$, $l \in \{1, 2, 3\}$ and $\nu \in \{1, 2, 3\}$. Moreover, the sample paths of the processes $\varepsilon^{1,l}$ and $\varepsilon^{2,l}$ have C^∞ sample paths, whereas the sample paths of $\varepsilon^{3,l}$, which is a Ornstein-Uhlenbeck process (e.g., Iacus (2009, p.43)), are only continuous, implying that the GKF is not applicable for this process.

From these error processes the generating Gaussian process A_t of the GP model is constructed by the following formula

$$A_t^{i,l,j,\sigma} = M_j (\sigma \varepsilon_{1,t}^{i,l}, \sigma \varepsilon_{2,t}^{i,l}, \sigma \varepsilon_{3,t}^{i,l})^T, \quad (19)$$

for $i \in \{1, 2, 3\}$, $j \in \{1, 2\}$, $l \in \{1, 2, 3\}$ and $\sigma \in \mathbb{R}_{>0}$. Here we denote with $\varepsilon_{s,t}^{i,l}$ for $s = 1, 2, 3$ independent realizations of $\{\varepsilon_t^{i,l}\}_{t \in I}$. The matrices

$$M_1 = \begin{pmatrix} 1 & 0 & 0 \\ 0 & 1 & 0 \\ 0 & 0 & 1 \end{pmatrix}, \quad M_2 = \begin{pmatrix} 1 & 0 & 0 \\ \frac{1}{2} & \frac{1}{2} & 0 \\ \frac{1}{\sqrt{3}} & \frac{1}{\sqrt{3}} & \frac{1}{\sqrt{3}} \end{pmatrix}.$$

are introduced to include correlations among the coordinates. Moreover, (19) introduces different variances in the coordinates, since for $j = 2$ the second component has half the variance of the other two components.

Design of simulation of simultaneous confidence tubes (SCTs) for center curves of GP models. First, $N \in \{10, 15, 30\}$ realizations of the process $\{A_t^{i,l,j,\sigma}\}$ on the equidistant time grid \mathcal{T} with $\Delta t = 0.01$ of $[0, 1]$ for $i \in \{1, 2, 3\}$, $j \in \{1, 2\}$, $l \in \{1, 2, 3\}$ and $\sigma \in \{0.05, 0.1, 0.6\}$ are simulated. We only report small sample sizes here, since the asymptotic behavior has been studied intensely in Telschow and Schwartzman (2019) and small simulation studies for higher sample sizes did not reveal departures from correct covering rates.

Then $(1 - \alpha)$ -SCT are constructed using Theorem 3.2. Here the quantile $\hat{h}_{\gamma, N, \alpha}$ is estimated by equation (16) using the estimator (17) for the Lipschitz killing curvature. Afterwards it is checked whether $\gamma_0 \equiv I_{3 \times 3}$ is contained in the SCT for all $t \in \mathcal{T}$. This procedure is repeated $M = 5000$ times. The true covering rate is approximated by the relative frequency of the numbers of simulations, in which the constructed SCT contained the true center curve γ_0 for all $t \in \mathcal{T}$.

Results of simulation of SCT for center curves of GP models. The results are reported in Table 1 and they convey a positive message: For a variance $\sigma = 0.05$, which is that of the data of the application in Section 6, the simulated covering rate is very close to $(1 - \alpha)$. Only in the case of the Ornstein-Uhlenbeck error process we have slightly too high covering rates. For higher variance ($\sigma = 0.6$) we underestimate the covering rate. This is expected, since the proposed estimator is designed for concentrated data and the map $v \mapsto \text{Log}(\text{Exp}(v))$ is only the identity on $\|v\| < \pi$ and we have the inequality

$$\left\| \text{Log}(\text{Exp}(v)) \right\|_F \leq \|v\|. \quad (20)$$

This implies that our estimated covariance matrix has smaller eigenvalues than the covariance matrix of the sample and hence our confidence sets will become smaller. This effect is more visible if the sample size is large, since more curves cross the cut locus.

N	σ	E.P.	$1 - \alpha$	$i = 1$	$i = 2$	$i = 3$
10	0.05	$A^{i,1,1,\sigma}$	85/90/95	86.1/91.0/95.0	85.3/90.1/95.6	90.4/93.9/96.6
15	0.05	$A^{i,1,1,\sigma}$	85/90/95	85.0/90.1/95.4	85.7/90.7/94.9	89.4/93.0/96.6
30	0.05	$A^{i,1,1,\sigma}$	85/90/95	85.1/91.0/94.9	86.4/90.6/94.7	90.1/93.5/96.5
10	0.05	$A^{i,1,2,\sigma}$	85/90/95	85.3/89.9/94.6	86.1/90.9/95.4	90.1/93.1/97.2
15	0.05	$A^{i,1,2,\sigma}$	85/90/95	85.4/89.8/95.4	85.9/90.5/94.9	90.3/93.0/96.7
30	0.05	$A^{i,1,2,\sigma}$	85/90/95	85.0/90.2/95.6	85.9/89.8/94.9	90.2/92.9/96.6
10	0.05	$A^{i,3,1,\sigma}$	85/90/95	84.8/90.0/95.3	86.2/90.9/95.5	91.0/93.6/97.1
15	0.05	$A^{i,3,1,\sigma}$	85/90/95	84.3/89.9/95.2	86.2/90.6/95.0	90.3/93.0/96.2
30	0.05	$A^{i,3,1,\sigma}$	85/90/95	84.7/90.1/95.2	86.6/90.8/94.9	90.0/92.6/96.5
10	0.05	$A^{i,3,2,\sigma}$	85/90/95	86.0/90.6/95.0	85.4/90.3/95.5	90.3/93.3/96.9
15	0.05	$A^{i,3,2,\sigma}$	85/90/95	84.9/90.0/94.7	85.4/90.5/95.3	90.1/93.5/97.3
30	0.05	$A^{i,3,2,\sigma}$	85/90/95	85.1/89.7/95.3	85.9/90.7/94.9	89.9/92.9/96.5
10	0.1	$A^{i,1,1,\sigma}$	85/90/95	84.7/90.8/94.9	85.2/91.4/95.4	90.3/93.4/96.7
15	0.1	$A^{i,1,1,\sigma}$	85/90/95	84.9/89.8/95.1	86.1/90.4/95.1	89.5/91.6/96.6
30	0.1	$A^{i,1,1,\sigma}$	85/90/95	85.0/90.5/95.1	85.8/91.1/95.5	89.9/92.7/96.3
10	0.1	$A^{i,1,2,\sigma}$	85/90/95	85.5/90.4/94.5	86.3/90.8/95.1	90.3/93.3/96.4
15	0.1	$A^{i,1,2,\sigma}$	85/90/95	85.4/89.9/94.7	86.1/89.9/95.3	89.9/93.1/95.9
30	0.1	$A^{i,1,2,\sigma}$	85/90/95	85.1/89.6/95.0	85.4/90.7/95.7	89.9/93.1/96.4
10	0.1	$A^{i,3,1,\sigma}$	85/90/95	85.4/90.1/96.0	85.4/90.2/94.6	90.1/93.6/97.0
15	0.1	$A^{i,3,1,\sigma}$	85/90/95	84.1/89.6/94.7	86.0/90.5/95.0	88.9/92.9/96.5
30	0.1	$A^{i,3,1,\sigma}$	85/90/95	85.4/90.3/94.9	85.3/90.1/95.3	88.9/93.4/96.5
10	0.1	$A^{i,3,2,\sigma}$	85/90/95	84.6/90.5/95.1	86.5/91.0/95.3	89.9/93.4/96.3
15	0.1	$A^{i,3,2,\sigma}$	85/90/95	85.2/90.2/95.1	86.2/89.8/95.3	89.8/93.1/96.2
30	0.1	$A^{i,3,2,\sigma}$	85/90/95	85.7/89.6/95.0	85.1/90.6/95.5	90.9/93.2/96.6
10	0.6	$A^{i,1,1,\sigma}$	85/90/95	82.4/87.7/93.9	81.6/87.3/93.6	87.1/91.2/95.5
15	0.6	$A^{i,1,1,\sigma}$	85/90/95	79.9/85.7/92.7	80.7/86.4/92.9	85.2/90.2/94.6
30	0.6	$A^{i,1,1,\sigma}$	85/90/95	79.4/85.5/92.4	78.7/84.8/92.3	82.8/87.6/92.9
10	0.6	$A^{i,1,2,\sigma}$	85/90/95	81.5/87.7/93.8	82.0/88.6/93.8	88.1/92.1/96.0
15	0.6	$A^{i,1,2,\sigma}$	85/90/95	81.9/86.8/93.1	81.0/87.1/93.2	86.3/90.5/94.7
30	0.6	$A^{i,1,2,\sigma}$	85/90/95	80.0/85.7/91.9	80.9/85.6/92.1	85.2/87.6/93.9
10	0.6	$A^{i,3,1,\sigma}$	85/90/95	83.0/88.7/94.7	84.2/88.8/94.2	88.1/91.6/96.0
15	0.6	$A^{i,3,1,\sigma}$	85/90/95	81.9/88.5/93.5	80.9/87.2/93.8	86.0/90.5/95.1
30	0.6	$A^{i,3,1,\sigma}$	85/90/95	80.2/86.7/93.1	80.0/86.3/92.8	85.0/89.5/94.0
10	0.6	$A^{i,3,2,\sigma}$	85/90/95	84.3/89.7/94.4	84.2/89.0/94.9	87.4/92.5/96.2
15	0.6	$A^{i,3,2,\sigma}$	85/90/95	81.5/86.8/93.5	81.6/87.2/94.0	86.2/89.7/95.2
30	0.6	$A^{i,3,2,\sigma}$	85/90/95	81.3/86.6/92.4	81.8/86.7/92.4	85.8/89.2/93.2

Table 1: Simulated covering rates (right box) of simultaneous $1 - \alpha$ -confidence tubes for GP models obtained from $M = 5000$ simulations for varying error processes (E.P.). Notably, the Ornstein-Uhlenbeck processes ($i = 3$) do not fulfill the assumptions necessary for application of the GKF.

6 Application: Assessing Kneeling Effects on Gait

Study design. In a study conducted at the School of Rehabilitation Science (McMaster University, Canada), 8 volunteers (4 female, 4 male, for each gender, two aged 20-30 and two aged 50-60) with no previous knee injuries (external observation and subjective questioning revealed no obvious knee problems) with unremarkable knee kinematics motion have been selected. In the experiment retro-reflective markers were placed onto identifiable skin locations on upper and lower volunteers' legs by an experienced technician following a standard protocol. Eight cameras recorded the position of the markers and from their motions, a moving orthogonal frame $E_u(t) \in SO(3)$ describing the rotation of the upper leg w.r.t. the laboratory's fixed coordinate system was determined, and one for the lower leg, $E_l(t) \in SO(3)$, each of which was aligned near $I_{3 \times 3}$ when the subject stood straight. As is common practice in clinical settings, subjects walked along a pre-defined 10 meter straight path at comfortable speed. For each of the following four sessions (A,B,C,D), for each subject a sample of $N \approx 12$ (for details on N , see Table 2) repeated walks have been conducted and for every walk a single gait cycle $\gamma(t) = E_u(t)E_l(t)^T$ about half way through has been recorded, representing the motion of the upper leg w.r.t. the lower leg. After each walk the volunteers stopped shortly and started again for the next 10 meter walk. Thus, by design the assumption of independence of recorded gait cycles is satisfied.

	0%	25%	50%	75%	100%
A	11.00	12.00	12.00	13.00	14.00
B	12.00	12.00	13.00	13.25	14.00
C	9.00	11.75	12.00	12.25	14.00
D	9.00	11.00	12.00	12.25	13.00

Table 2: Reporting the quartiles of numbers of processed walks (gait cycles) of volunteers for each of the four sessions from Table 3.

The study consists of four sessions, each giving, as described above, a sample of walks for the left leg of each volunteer. Between samples *A* and *B* the markers were detached and placed again by the same technician following the same standard protocol. Hence the difference between these samples reflects the challenge of repeated reproducibility of gait patterns under clinical conditions. Before conducting the two sessions *C* and *D* markers were again replaced and the volunteers fulfilled a task of 15 minutes kneeling prior to data collection of session *C* and yet another 15 minutes kneeling prior to session *D*. This allows to study the effect of kneeling and prolonged kneeling on gait patterns. Table 3 gives an overview of the four sessions conducted. Sessions *A* and *B* have already been reported in Telschow et al. (2016).

Session	explanation
A	no intervention, walks
B	no intervention but marker replacement, walks
C	marker replacement, 15 minutes of moderate kneeling, walks
D	no marker replacement, another 15 minutes of prolonged kneeling, walks

Table 3: Experiments conducted

Dealing with the marker replacement effect. Replacing markers between sessions results in fixed and different rotations of the upper and lower leg, conveyed by suitable $P, Q \in SO(3)$ such that $E_u^{\text{after}}(t) = PE_u^{\text{before}}(t)$ and $E_l^{\text{after}}(t) = Q^TE_l^{\text{before}}(t)$. Estimation of P and Q and temporal alignment of the sample mean curves have been done as described in Section 2 and detailed in Telschow et al. (2016) in order to make the samples comparable. Indeed, by Theorem 4.5 the shape of the confidence sets does not depend on alignment correction.

In the following we report our findings, first in Table 4 using the permutation test from Telschow et al. (2016, Test 2.11) correcting for sample-specific group action. If we were not to correct for sample-specific group action, we would detect significant changes of gait for 6 out of the 8 volunteers, even for “A vs. B”, where nothing changed but marker placement, cf. Telschow et al. (2016, Table 2) . The challenge dealt with in Telschow et al. (2016) was to design a test keeping the level, also under marker replacement.

Vol	A vs. C	B vs. C	A vs. D	B vs. D
1	0.204	0.158	0.029	0.127
2	0.046	0.002	0.0	0.0
3	0.872	0.307	0.191	0.311
4	0.001	0.001	0.0	0.0
5	0.214	0.735	0.559	0.355
6	0.0	0.0	0.001	0.008
7	0.0	0.0	0.027	0.042
8	0.467	0.705	0.102	0.149

Table 4: Reporting p -values (significant in bold face) obtained from the permutation test in Telschow et al. (2016, Test 2.11 in the version of Remark 2.12) correcting for sample-specific group action.

Results. In Table 4, we see significant (often highly significant) changes of gait of volunteers 2, 4, 6 and 7 after each of the kneeling tasks. Volunteers 3, 5 and 8 show no changes. Remarkably, these findings are consistent over marker replacement (“A vs. *” and “B vs. *”) and only for Volunteer 1 the picture is unclear.

In order to locate changes of gait patterns, we apply our new test of simultaneous confidence tubes. In Table 5 we report the specific loci where $1 - \alpha = 0.95$ confidence tubes no longer overlap, using standard naming convention (e.g. Rodgers (1995)) as illustrated in Figure 1. Employing Euler angles, which are popular in the field, as a local chart of $SO(3)$, the corresponding curves and specific loci of non-overlapping simultaneous confidence tubes are shown exemplary in Figures 2 for Volunteer 2 and in Figure 3 for Volunteer 6. Notably, non-overlapping confidence tubes have been determined in $SO(3)$ and not in chart coordinates so that the chart representations only serve as an approximate visualization of the real situation which we cannot visualize. The other volunteers’ (1, 3, 4 and 7) curves with loci of non-overlapping confidence tubes are shown in the appendix in Figure 4. Again, we see that Volunteers 5 and 8 feature no changes in gait pattern. Volunteer 7 reported physical pain after post-kneeling walking. Indeed, high variation in gait patterns corresponding to session D (red, in the left two displays of the bottom row in Figure 4) widened the corresponding confidence tubes such that changes of gait in Session D were not detected.

Combining Tables 4 and 5 and taking into account age and gender, we see that older age (volunteers with even numbers belong to age group 50 - 60) favors a kneeling effect over young age (volunteers with odd numbers belong to age group 20 - 30). As a surprise, the effect seems to be overall stronger for males. Having established a tool chain to study such effects, this experiment warrants larger studies.

7 Discussion

In conjunction with the permutation test and estimation of marker replacement effects from Telschow et al. (2016), with the test for simultaneous non-overlapping confidence tubes presented in this paper, we have developed a tool chain that can be used in clinical practice to assess changes of gait patterns and localize these. These are no longer based on (single) Euler angle representations, as are often used in the field, but take advantage of a Gaussian perturbation model defined

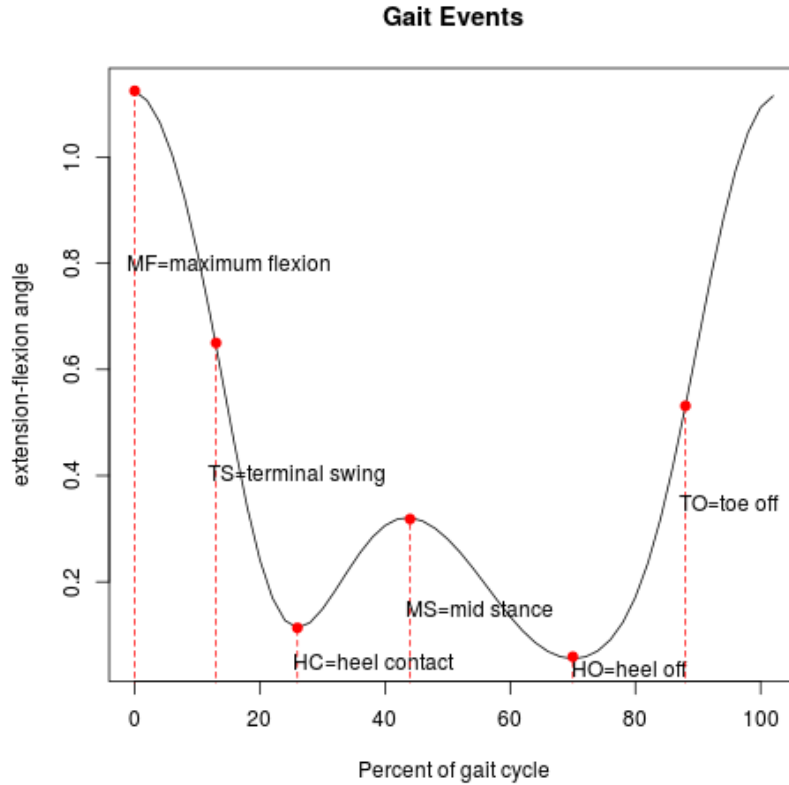


Figure 1: *Depicting standard naming convention for gait events with respect to the flexion-extension angle.*

Vol.	A vs. C	B vs. C	A vs. D	B vs. D	gender	age group
1				MS	m	20-30
2	HC	TS, HC, HO-TO	TS,HC,TO	TS, HC, HO-TO, MF	m	50-60
3			HC		f	20-30
4			TS	TS	f	50-60
5					m	20-30
6	TO	HO		HO	m	50-60
7		HC			f	20-30
8					f	50-60

Table 5: *Events from Figure 1 where gait patterns changed such that 0.95-confidence tubes no longer overlap.*

in the Lie group of three dimensional rotations. Due to the conservation of moment, gait curves are naturally smooth, their variation over repeated walks is moderate and hence approximations via the Gaussian kinematic formula are rather accurate, as well as in theory as in practice.

In this study, with a small number of participants and a small number of repeated walks, we see that short kneeling tasks tend to affect gait patterns and it seems that older age and, possibly, male gender, favor this effect. We have made sure that this effect has not been caused by different marker placements. While specific loci of gait change depend on individuals, changes seem to occur least at local maxima of dominating flexion-extension, namely at MF and MS.

We believe that our results derived for $G = SO(3)$ generalize to general connected Lie groups

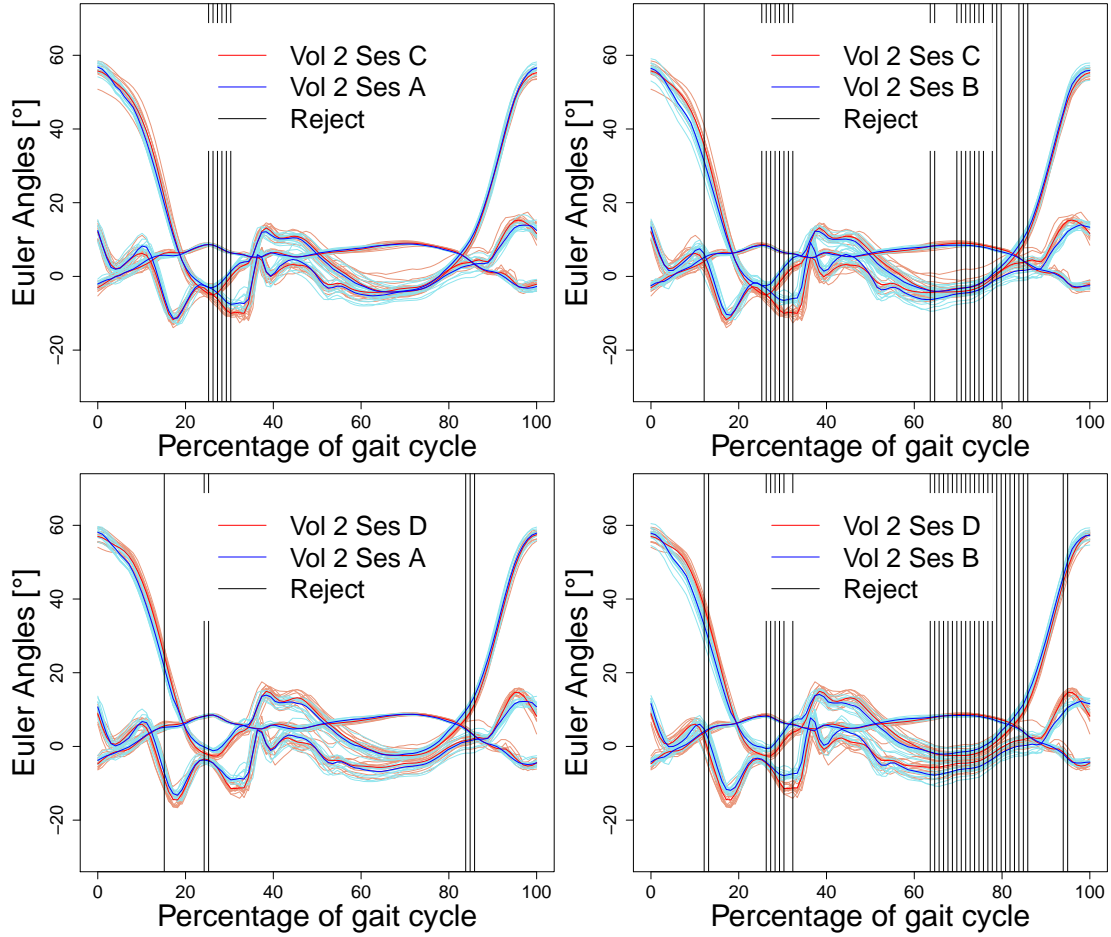


Figure 2: *Depicting for Volunteer 2 all three Euler angles of sampled gait curves for each of two different sessions. PEM curves are fat and vertical lines indicate loci of non-overlapping simultaneous 0.05-confidence tubes in $SO(3)$. The largely varying curves are flexion-extension angles, cf. Figure 1, the middle curves with least variation are abduction-adduction and the bottom ones are internal-external angles.*

setting as introduced in Sections 2 and 3, in particular to products of $SO(3)$ with itself and with the Euclidean motion group, which are used in biomechanical analysis of more complicated joints (e.g. Rivest et al. (2008) for ankle motion) and in motion analysis of *kinematic chains* of entire limbs (e.g. Laitenberger et al. (2015)) and their design for humanoid robots (e.g. Ude et al. (2004)).

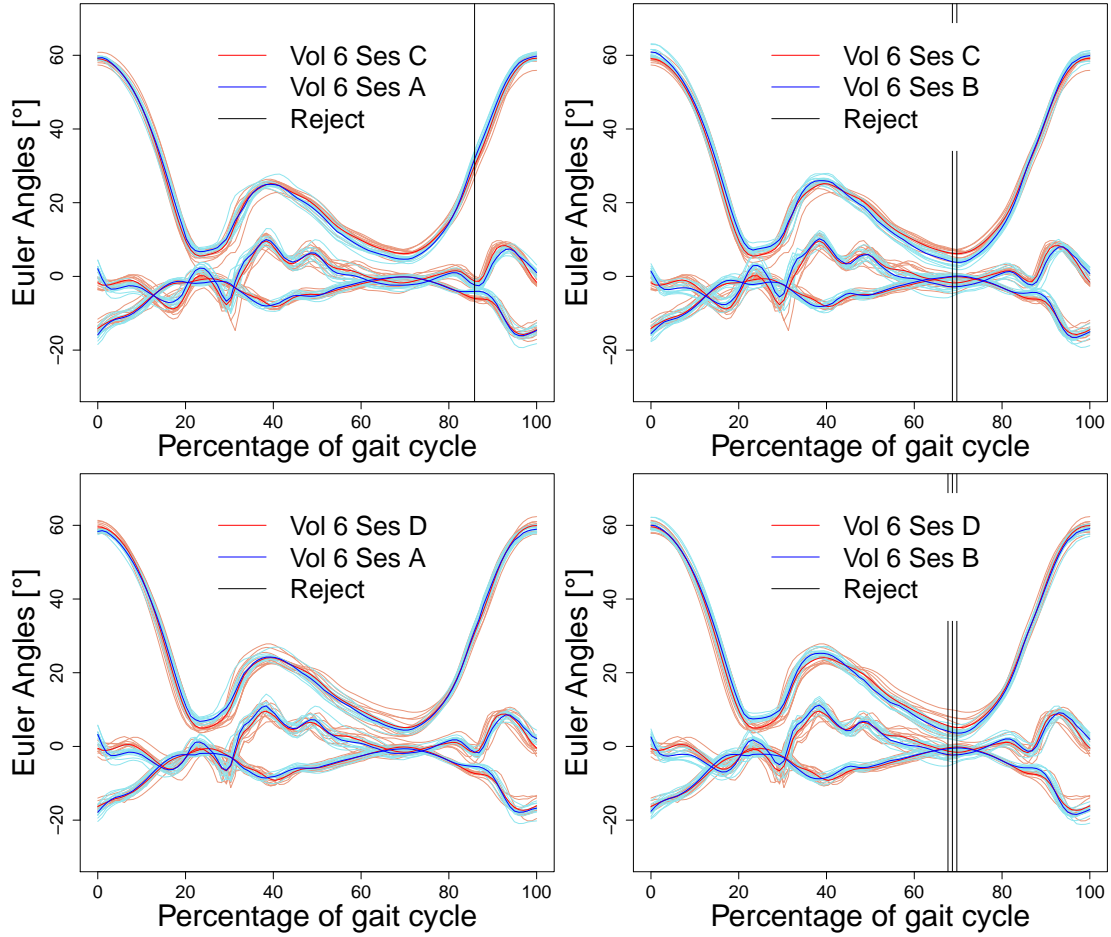


Figure 3: *Depicting with notation from Figure 2 for Volunteer 6 all three Euler angles of sampled gait curves for each of two different sessions with PEM curves and loci of non-overlapping simultaneous 0.05-confidence tubes in $SO(3)$.*

8 Acknowledgements

The first and the second author gratefully acknowledge support from DFG HU 1575/4 and 1575/7, the Niedersachsen Vorab of the Volkswagen Foundation and DFG GRK 2088.

References

- Bhattacharya, R. N. and V. Patrangenaru (2003). Large sample theory of intrinsic and extrinsic sample means on manifolds I. *The Annals of Statistics* 31(1), 1–29.
- Chirikjian, G. S. and A. B. Kyatkin (2000). *Engineering applications of noncommutative harmonic analysis: with emphasis on rotation and motion groups*. CRC press.
- Coggon, D., P. Croft, S. Kellingray, D. Barrett, M. McLaren, and C. Cooper (2000). Occupational physical activities and osteoarthritis of the knee. *Arthritis & Rheumatism: Official Journal of the American College of Rheumatology* 43(7), 1443–1449.
- Cooper, C., T. McAlindon, D. Coggon, P. Egger, and P. Dieppe (1994). Occupational activity and osteoarthritis of the knee. *Annals of the rheumatic diseases* 53(2), 90–93.

- Delval, A., J. Salleron, J.-L. Bourriez, S. Bleuse, C. Moreau, P. Krystkowiak, P. D. Luc Defebvre and, and A. Duhamel (2008). Kinematic angular parameters in PD: Reliability of joint angle curves and comparison with healthy subjects. *Gait and Posture* 28, 495 – 501.
- Duhamel, A., J. Bourriez, P. Devos, P. Krystkowiak, A. Destee, P. Derambure, and L. Defebvre (2004). Statistical tools for clinical gait analysis. *Gait & posture* 20(2), 204–212.
- Gaudreault, N., N. Hagemester, S. Poitras, and J. A. de Guise (2013). Comparison of knee gait kinematics of workers exposed to knee straining posture to those of non-knee straining workers. *Gait & posture* 38(2), 187–191.
- Henderson, H. V. and S. R. Searle (1981). On deriving the inverse of a sum of matrices. *Siam Review* 23(1), 53–60.
- Iacus, S. M. (2009). *Simulation and inference for stochastic differential equations: with R examples*. Springer Science & Business Media.
- Kadaba, M., H. Ramakrishnan, M. Wootten, J. Gainey, G. Gorton, and G. Cochran (1989). Repeatability of kinematic, kinetic, and electromyographic data in normal adult gait. *Journal of Orthopaedic Research* 7(6), 849–860.
- Kajaks, T. and P. Costigan (2015). The effect of sustained static kneeling on kinetic and kinematic knee joint gait parameters. *Applied ergonomics* 46, 224–230.
- Laitenberger, M., M. Raison, D. Périé, and M. Begon (2015). Refinement of the upper limb joint kinematics and dynamics using a subject-specific closed-loop forearm model. *Multibody System Dynamics* 33(4), 413–438.
- McGinley, J. L., R. Baker, R. Wolfe, and M. E. Morris (2009). The reliability of three-dimensional kinematic gait measurements: a systematic review. *Gait & posture* 29(3), 360–369.
- Mecke, K. R. and D. Stoyan (2000). *Statistical physics and spatial statistics: the art of analyzing and modeling spatial structures and pattern formation*, Volume 554. Springer Science & Business Media.
- Noehren, B., K. Manal, and I. Davis (2010). Improving between-day kinematic reliability using a marker placement device. *Journal of Orthopaedic Research* 28(11), 1405–1410.
- Rancourt, D., L.-P. Rivest, and J. Asselin (2000). Using orientation statistics to investigate variations in human kinematics. *Applied Statistics*, 81–94.
- Rivest, L.-P., S. Baillargeon, and M. Pierrynowski (2008). A directional model for the estimation of the rotation axes of the ankle joint. *Journal of the American Statistical Association* 103(483), 1060–1069.
- Rodgers, M. M. (1995). Dynamic foot biomechanics. *Journal of Orthopaedic & Sports Physical Therapy*, 306–316.
- Røislien, J., Ø. Skare, A. Opheim, and L. Rennie (2012). Evaluating the properties of the coefficient of multiple correlation (cmc) for kinematic gait data. *Journal of biomechanics* 45(11), 2014–2018.
- Rytter, S., N. Egund, L. K. Jensen, and J. P. Bonde (2009). Occupational kneeling and radiographic tibiofemoral and patellofemoral osteoarthritis. *Journal of Occupational Medicine and Toxicology* 4(1), 19.
- Rytter, S., L. K. Jensen, J. P. Bonde, A. G. Jurik, and N. Egund (2009). Occupational kneeling and meniscal tears: a magnetic resonance imaging study in floor layers. *The Journal of rheumatology* 36(7), 1512–1519.

- Srivastava, A., W. Wu, S. Kurtek, E. Klassen, and J. Marron (2011). Registration of functional data using fisher-rao metric. *arXiv preprint arXiv:1103.3817*.
- Su, J., S. Kurtek, E. Klassen, A. Srivastava, et al. (2014). Statistical analysis of trajectories on riemannian manifolds: bird migration, hurricane tracking and video surveillance. *The Annals of Applied Statistics* 8(1), 530–552.
- Taylor, J., A. Takemura, and R. J. Adler (2005). Validity of the expected euler characteristic heuristic. *Annals of Probability*, 1362–1396.
- Taylor, J. and K. Worsley (2008). Random fields of multivariate test statistics, with applications to shape analysis. *Ann. Statist.*, 1–27.
- Taylor, J. E. (2006). A Gaussian kinematic formula. *The Annals of Probability* 34(1), 122–158.
- Taylor, J. E. and K. J. Worsley (2007). Detecting sparse signals in random fields, with an application to brain mapping. *Journal of the American Statistical Association* 102(479), 913–928.
- Telschow, F. J., S. F. Huckemann, and M. R. Pierrynowski (2016). Functional inference on rotational curves and identification of human gait at the knee joint. *arXiv preprint arXiv:1611.03665*.
- Telschow, F. J. and A. Schwartzman (2019). Simultaneous confidence bands for functional data using the gaussian kinematic formula. *arXiv preprint arXiv:1901.06386*.
- Tennant, L., D. Kingston, H. Chong, and S. Acker (2015). The effect of work boots on knee mechanics and the center of pressure at the knee during static kneeling. *Journal of applied biomechanics* 31(5), 363–369.
- Tennant, L. M., H. C. Chong, and S. M. Acker (2018). The effects of a simulated occupational kneeling exposure on squat mechanics and knee joint load during gait. *Ergonomics* 61(6), 839–852.
- Ude, A., C. G. Atkeson, and M. Riley (2004). Programming full-body movements for humanoid robots by observation. *Robotics and autonomous systems* 47(2-3), 93–108.
- Wilkins, K. J., L. V. Duong, M. H. McGarry, W. C. Kim, and T. Q. Lee (2007). Biomechanical effects of kneeling after total knee arthroplasty. *JBJs* 89(12), 2745–2751.

A Appendix: More Visualizations of the Test for Non-Overlapping Confidence Tubes

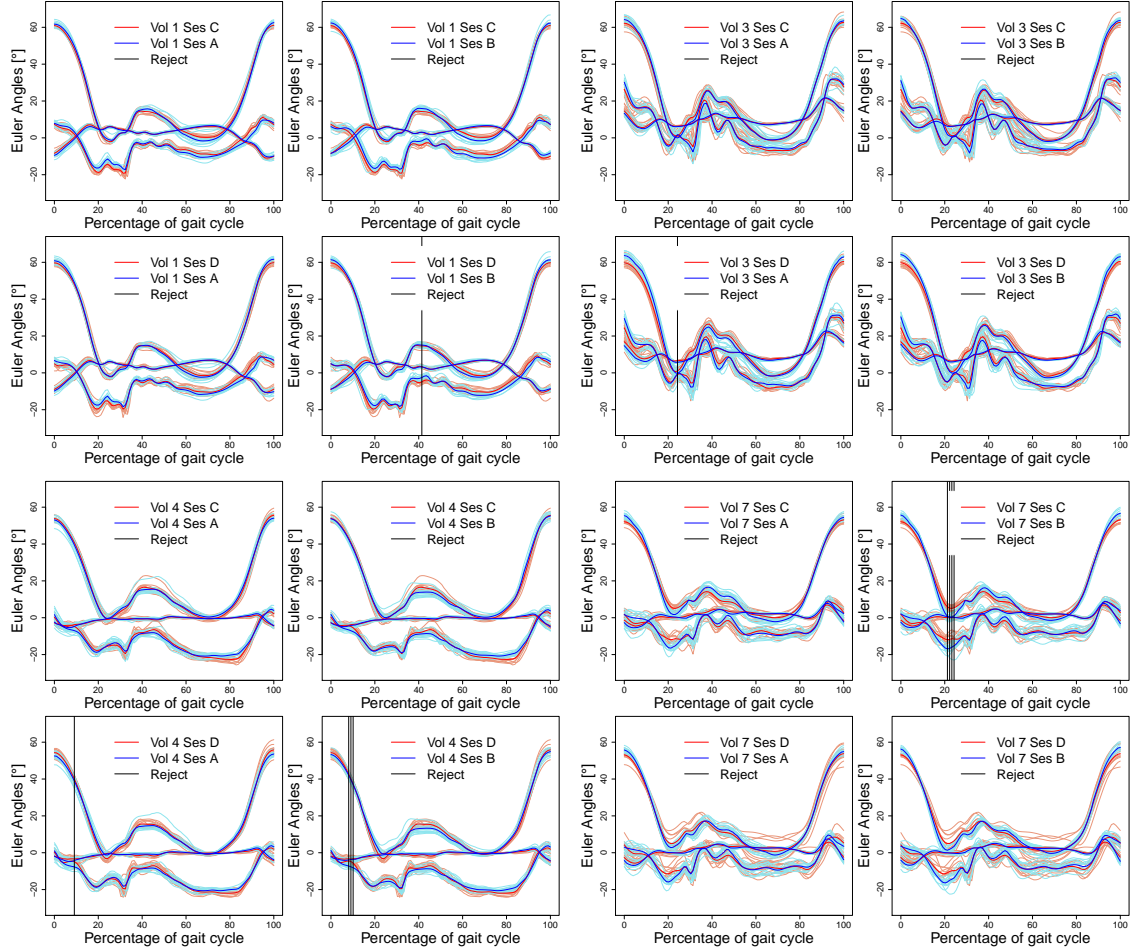


Figure 4: *Depicting with notation from Figure 2 for Volunteers 1, 3, 4 and 7 all three Euler angles of sampled gait curves for each of two different sessions with PEM curves and loci of non-overlapping simultaneous 0.05-confidence tubes in $SO(3)$.*

B Appendix: Proofs

Proof of Theorem 4.3 Consider samples $\gamma_1, \dots, \gamma_N$ with fixed $N \in \mathbb{N}$ of a GP model $\gamma_0 \text{Exp}(A_t)$ with $a_t = \iota^{-1} \circ A_t$, $\max_{t \in [0,1]} \|a_t\| = \mathcal{O}_p(\sigma)$ and $\sigma \rightarrow 0$, and let $\hat{\gamma}_N(t) \in E_N(t)$ be a measurable selection of PEMs. Then for each $t \in [0, 1]$, taking $x_t^N \in \mathbb{R}^3$ from Definition 3.1 and $X_t^N = \iota \circ x_t^N$ we have that $\hat{\gamma}_N(t) = \gamma_0 \text{Exp}(X_t^N)$. Moreover, making use of the fact

$$\left(\iota \left(\frac{x}{\|x\|} \right) \right)^2 = \frac{xx^T}{\|x\|^2} - I_{3 \times 3}. \quad (21)$$

the property, $\text{trace}(\iota(c)^T \iota(d)) = 2c^T d$ for all $c, d \in \mathbb{R}^3$, and the Rodriguez formula (9), we have for each $t \in [0, 1]$ that X_t^N maximizes

$$\begin{aligned} & \frac{1}{N} \sum_{n=1}^N \text{trace} \left(\hat{\gamma}_N^T(t) \gamma_0(t) \text{Exp}(A_t^n) \right) \\ &= \text{trace} \left(\left(I_{3 \times 3} + \iota(x_t^N) \text{sinc}(\|X_t^N\|_F) + \frac{1 - \cos(\|X_t^N\|_F)}{\|X_t^N\|_F^2} \iota(x_t^N)^2 \right)^T \right. \\ & \quad \left. \cdot \left(I_{3 \times 3} + \iota(\bar{a}_t^N) + \mathcal{O}_p(\sigma^2) \right) \right) \\ &= 3 + \text{trace} \left(\iota(x_t^N)^T \iota(\bar{a}_t^N) \text{sinc}(\|x_t^N\|) + (1 - \cos(\|x_t^N\|)) \left(\iota \left(\frac{x_t^N}{\|x_t^N\|} \right) \right)^2 + \mathcal{O}_p(\sigma^2) \right) \\ &= 1 + 2 \left(x_t^{N^T} \bar{a}_t^N \text{sinc}(\|x_t^N\|) + \cos(\|x_t^N\|) \right) + \mathcal{O}_p(\sigma^2). \end{aligned}$$

Note that the $\mathcal{O}_p(\sigma^2)$ is indeed uniform in $t \in [0, 1]$.

Writing $x_t^N = re$ with a unit vector e and length $0 \leq r \leq \pi$, the first two summands above are maximized in x_t^N if

$$s \sin(r) + \cos(r)$$

is maximal under the side condition $-\|\bar{a}_t^N\| \leq s = e^T \bar{a}_t^N \leq \|\bar{a}_t^N\|$. Hence, for $0 \leq r < \pi$ choose the maximizing $s = \|\bar{a}_t^N\|$ (as large as possible) and hence $r = \arctan(\|\bar{a}_t^N\|) \in (0, \pi/2)$ ($r = \pi$ is no option). In consequence we have that

$$x_t^N = \bar{a}_t^N \frac{\arctan \|\bar{a}_t^N\|}{\|\bar{a}_t^N\|} + \mathcal{O}_p(\sigma^2) = \bar{a}_t^N + \mathcal{O}_p(\sigma^2).$$

This is (12).

To establish equation (13) from the above, consider the Taylor expansion

$$\begin{aligned} x_t^{N,n} &= \mathfrak{L} \left(\hat{\gamma}_N^T(t) \gamma_n(t) \right) = \iota^{-1} \circ \text{Log} \left(\text{Exp} \left(-\iota \circ \bar{a}_t^N + \mathcal{O}_p(\sigma^2) \right) \text{Exp} \left(\iota \circ a_t^n \right) \right) \\ &= a_t^n - \bar{a}_t^N + \mathcal{O}_p(\sigma^2) \end{aligned}$$

wich is not valid for $\|a_t^n - x_t^N\| \geq \pi$, cf. Chirikjian and Kyatkin (2000, p. 121). The probability of which, however, is $\mathcal{O}(\sigma^2)$, uniformly over $t \in [0, 1]$, yielding the second assertion. \square

Proof of Corollary 4.4 Recall the definitions

$$H_t^{a,N} = N(\bar{a}_t^N)^T \left(S_t^{a,N} \right)^{-1} \bar{a}_t^N \quad \text{and} \quad \tilde{H}_t^{x,N} = N(x_t^N)^T \left(\hat{S}_t^{x,N} \right)^{-1} x_t^N.$$

By virtue of Theorem 4.3 we obtain

$$\hat{S}_t^{x,N} = S_t^{a,N} + Z_t$$

with $\max_t \|Z_t\|_F = \mathcal{O}_p(\sigma_l^3)$. Using Henderson and Searle (1981, p. 58, eq. (24)) yields

$$\begin{aligned} \frac{1}{N} \hat{H}_t^{x,N} &= (x_t^N)^T \left(S_t^{a,N} + Z_t \right)^{-1} x_t^N \\ &= (x_t^N)^T \left(S_t^{a,N} \right)^{-1} x_t^N - (x_t^N)^T \left(S_t^{a,N} \right)^{-1} Z_t \left(I_{3 \times 3} + \left(S_t^{a,N} \right)^{-1} Z_t \right)^{-1} \left(S_t^{a,N} \right)^{-1} x_t^N. \end{aligned}$$

From the assumption $\text{var}[a_t^n] = \sigma^2 \Sigma_t$ we have that $\max_{t \in [0,1]} \left\| (S_t^{a,N})^{-1} \right\|_F = \mathcal{O}_p(\sigma^{-2})$. Thus, we obtain

$$(x_t^N)^T (S_t^{a,N})^{-1} x_t^N = \frac{1}{N} H_t^{a,N} + \mathcal{O}_p(\sigma)$$

by equation (12). Moreover, we obtain that $\max_{t \in [0,1]} \left\| (S_t^{a,N})^{-1} Z_t \right\|_F = \mathcal{O}_p(\sigma)$ implying $(S_t^{a,N})^{-1} Z_t \xrightarrow{\mathbb{P}} 0$ uniformly over $t \in [0,1]$. In consequence, on $U = \left\{ \left\| (S_t^{a,N})^{-1} Z_t \right\|_F < 1 \right\}$ we have the Von Neumann series

$$\left(I_{3 \times 3} + (S_t^{a,N})^{-1} Z_t \right)^{-1} = \sum_{j=0}^{\infty} (-1)^j \left((S_t^{a,N})^{-1} Z_t \right)^j$$

showing at once

$$(x_t^N)^T (S_t^{a,N})^{-1} Z_t \left(I_{3 \times 3} + (S_t^{a,N})^{-1} Z_t \right)^{-1} (S_t^{a,N})^{-1} x_t^N = \mathcal{O}_p(\sigma).$$

Since $\mathbb{P}\{U\} = 1 - \mathcal{O}(\sigma)$, this completes the proof. \square

Proof of Theorem 4.5. With the intrinsic residuals for each of the samples:

$$x_t^{N,n} = \mathfrak{L}\left(\hat{\gamma}_N^T(t) \gamma_n(t)\right) \quad \text{and} \quad y_t^{N,n} = \mathfrak{L}\left(\hat{\eta}_N^T(t) \eta_n(t)\right),$$

due to equivariance, $\hat{\eta}_N = \psi \circ \hat{\gamma}_N \circ \phi$, setting $\psi(R) = P_\psi R Q_\psi$ with $R, P_\psi, Q_\psi \in SO(3)$, we have

$$\begin{aligned} y_t^{N,n} &= \iota^{-1} \circ \text{Log}\left(Q_\psi^T \hat{\gamma}_N^T(\phi(t)) \gamma_n(\phi(t)) Q_\psi\right) \\ &= \pm \iota^{-1} \left(Q_\psi^T \text{Log}\left(\hat{\gamma}_N^T(\phi(t)) \gamma_n(\phi(t))\right) Q_\psi \right) \\ &= \pm Q_\psi \iota^{-1} \circ \text{Log}\left(\hat{\gamma}_N^T(\phi(t)) \gamma_n(\phi(t))\right) \\ &= \pm Q_\psi x_{\phi(t)}^{N,n}. \end{aligned}$$

Here, the second equality is due to the power series expansion of the matrix logarithm and the observation that different extensions of the matrix logarithm to the cut locus of $I_{3 \times 3}$ differ only by their sign; the third equality is due to (8). Moreover, by a similar argument for $x_t^N = \mathfrak{L}\left(\hat{\gamma}_N^T(t) \gamma_0(t)\right)$ and $y_t^N = \mathfrak{L}\left(\hat{\eta}_N^T(t) \eta_0(t)\right)$ we obtain $y_t^N = \pm Q_\psi x_{\phi(t)}^N$, yielding

$$\hat{S}_t^{y,N} = Q_\psi \hat{S}_{\phi(t)}^{x,N} Q_\psi^T, \quad \hat{H}_t^{y,N} = \hat{H}_{\phi(t)}^{x,N} \quad \text{and} \quad \hat{h}_{\gamma,N,\beta} = \hat{h}_{\eta,N,\beta}.$$

This implies $\mathcal{V}_\beta((\eta_1, \dots, \eta_N); t) = Q_\psi \mathcal{V}_\beta(\gamma_1, \dots, \gamma_N; \phi(t))$, yielding the assertion. \square